Article

Journal of Vibration and Control
2024, Vol. 30(11-12) 2647–2660

DOI: 10.1177/10775463231182462
journals.sagepub.com/home/jvc
Sage

An adaptive impedance control for dual-arm manipulators incorporated with the virtual decomposition control

Xin Jing[1], Loris Roveda[2], Jianfei Li[3], Yaobing Wang[3], and Haibo Gao[1]

Abstract

The interaction force control problem for the object manipulated by the dual-arm manipulator with the unknown environment is addressed in this paper. An adaptive dual-loop impedance control scheme is designed to meet the three control targets, including the trajectory tracking control of the object, the internal force control of the object with the two arms, and the interaction force control of the object with the unknown environment. Firstly, an adaptive variable impedance control method is proposed in the outer loop to copy with the unknown stiffness and position of the environment. Secondly, an impedance control scheme based on the internal force is designed in the inner loop to plan the internal force and the modified position supplied with the outer-loop control. Thirdly, to realize the reference trajectory supplied with the inner-loop control, the virtual decomposition control (VDC) method is incorporated, which is a recursive adaptive control progress, so that the unknown dynamics of the manipulators is acceptable and the computation complexity is also very low to satisfy the real-time control requirement. The stability verifications of the inner-loop impedance control and the VDC method are given based on the Lyapunov method, and the stability analysis of the outer-loop impedance control is obtained using the Routh criterion. Finally, a plane dual-arm robotic manipulator with three degrees of freedom is used to verify the effectiveness of the proposed control scheme.

Keywords

Dual-arm manipulator, impedance control, virtual decomposition control, adaptive control, force control, dual-loop impedance

1. Introduction

In the recent 40 years, the dual-arm robotic manipulator has been obtained large amount of attention by the researchers, ranging from transporting a common object, assembly, interacting with the environment and so on (Smith et al., 2012). The main reason why so many tasks are resolved by two arms or even more arms is that dual-arm robotic manipulator can finish tasks as the human does (Weng et al., 2019). However, the control issues reflected in the dual-arm system seem more complicated than a single manipulator, whether it is the position control or the force control. The control problems have been well addressed in the springer handbook of robotics (Caccavale and Uchiyama, 2016), such as the master/slave control scheme (Luh and Zheng, 1987; Jiao et al., 2022), the position/force hybrid control scheme (Uchiyama and Dauchez, 1988), the feedback linearization control scheme (Ping, 1992), the impedance control scheme (Bonitz and Hsia, 1996a; Caccavale et al., 2008), and the synchronization control scheme (Dong and Mills, 2002; Rodriguez-Angeles and Nijmeijer, 2004; Zhai et al., 2021). However, the addressed problem in this paper will be focusing on the modifications of the dual-loop

[1]State Key Laboratory of Robotics and Systems, Harbin Institute of Technology, Harbin, China
[2]Istituto Dalle Molle di studi sull'Intelligenza Artificiale (IDSIA), Scuola Universitaria Professionale della Svizzera Italiana (SUPSI), Università della Svizzera italiana (USI), Lugano, Switzerland
[3]Beijing Key Laboratory of Intelligent Space Robotic Systems Technology and Applications, Beijing Institute of Spacecraft System Engineering, Beijing, China

Received: 6 December 2022; accepted: 29 May 2023

Corresponding author:
Yaobing Wang, Beijing Key Laboratory of Intelligent Space Robotic Systems Technology and Applications, Beijing Institute of Spacecraft System Engineering, Beijing 10094, China.
Email: iamwyb@163.com

impedance control scheme, which has been widely used in the existing papers(Caccavale et al., 2008; Heck et al., 2013; Ren et al., 2016; He et al., 2016; Jinjun et al., 2019; Hu and Cao, 2022; Song et al., 2021). So that the literature review in this paper will be divided into two aspects: one is that only the transportation of the manipulated object is considered, and another is that the object will be interacted with the environment meanwhile.

1.1. Only transportation

Compared with a single manipulator operating in the free space, the position of the object and the internal force between the object and the end-effectors are needed to be controlled simultaneously in the dual-arm system, due to the fact that the position tracking errors can cause undesired internal force. The well-known the internal force-based impedance was proposed to address the above control requirements, which avoids the consideration of the dynamics of the object into the control scheme, and only the kinematics are needed to compute the internal force (Bonitz and Hsia, 1996a). However, the above model-based scheme is critically dependent on knowledge of the manipulator dynamics, so that a robust auxiliary controller was proposed by the same authors, which is still weakly dependent on each arm's inertia matrix (Bonitz and Hsia, 1996b). A fractal impedance control was proposed to adapt to multiple cooperative scenarios which exploits its non-linear stiffness (Babarahmati et al., 2021). Recently, a non-linear stiffness adaptation was also proposed to realize more robust grasp, and an energy tank-based method was used to verify the passivity (Shahriari et al., 2022). A master/slave scheme was used in the dual-arm cooperation, and a variable stiffness of the slave arm was designed to copy with the uncertainty of the stiffness and position of the object (Jiao et al., 2022). In this paper, it is assumed that the kinematics relationship of the rigid object and the two arms is invariable as in (Bonitz and Hsia, 1996a).

1.2. Interaction meanwhile

Apart from the transportation task above, sometimes the object is required to interact with the environment, such as applying a desired force on the environment. A dual-loop impedance control scheme is usually proposed to solve the two problems meanwhile, such as the work presented in (Caccavale et al., 2008), where, the impedance parameters are all invariable, and the low-level position control method used a simple PID control scheme. Similar with the above work, the work proposed by Heck complements the asymptotic stability analysis of (Khalil, 1996), and the motion controller is a "PD+" control method, which assumed that the dynamics of the manipulators are known (Heck et al., 2013). A biomimetic object impedance control was proposed to copy with the disturbances, the adaptation of the damping and stiffness relies on the deviations of the position and velocity of the object, the position controller is also a "PD+" control method (Ren et al., 2016). A variable impedance control relies on the deviation of the force acting on the environment was proposed, and to copy with the unknown dynamics of the manipulators, a sliding mode controller was used in the low-level position control (He et al., 2016). A kind of adaptive variable impedance control scheme based on the force deviation has been proposed to modify the reference trajectory to copy with the uncertainties of the stiffness and position of the environment (Song et al., 2021; Hu and Cao, 2022; Jinjun et al., 2019), however, the above three methods consider only adaptation of the stiffness or the damping, and the low-level position controllers all relies on the servo system of the manipulators. A projected inverse dynamics framework was established in the dual-arm cooperation, an external impedance controller is incorporated within the unconstrained subspace to copy with the external disturbances, and the contact force within the constrained subspace was optimized to against the external disturbance (Lin et al., 2018).

The virtual decomposition control (VDC) method is a recursive adaptive control scheme, which has been used in many different robots and scenarios (Zhu, 2010). An adaptive force/position controller for cooperation manipulation based on the VDC was proposed (Zhu and De Schutter, 1999, 2002), even in the flexible-joint multi-arm system (Zhu et al., 1998). Although the VDC has been used in the impedance control (Koivumäki and Mattila, 2016), however, to the authors' knowledge, there is not a paper that ever used the VDC in the internal force-based impedance control scheme for dual-arm system.

The main contributions reflected in two aspects: one is that the VDC method is the first time to be incorporated within the internal force-based impedance scheme, due to the VDC method contains two parts for the rigid-joint manipulators, the first one is the links dynamics control, and the second one is the joints dynamics control, for an actuated joint, the feedback control part plus the estimated torque bias can be equivalent to a joint PID control (Zhu, 2010), so that the servo control or the "PD+" control in most of the dual-loop control schemes can be seen as the special cases for the VDC method. Moreover, the link dynamics control part in the VDC method can enhance the position tracking performance and reduce the control effort due to its adaptation to the dynamic model of the manipulators. Because of the recursion process in the VDC, so that its computational complexity is lower than the most of the model-based control methods in the low-level position control. Another contribution is that a modified adaptive impedance control method in the outer loop is proposed, compared with the controllers in Song et al. (2021; Hu and Cao (2022; Jinjun et al. (2019), a dynamics adjustment of the damping is added in this paper to reduce the vibration in the contact stage.

This paper is organized as follows: In the *Dual-arm system section*, the necessary kinematics and dynamics (including the arms and the object) are established. In the *Dual-loop control scheme section*, the overall control scheme, a modified dual-loop impedance control method is proposed. Stability analysis is presented in detail in *Stability analysis section*. To verify the effectiveness of the proposed controller, a plane dual-arm robotic manipulator is used in *Simulation section*. Finally, the conclusion is given.

2. Dual-arm system

In this section, the kinematics and dynamics of the dual-arm system are given, as shown in Figure 1, the system contains two manipulators, denoted by Arm-a and Arm-b, and the rigid object manipulated by the two arms coordinately.

In Figure 1, some important frames are given, $\sum_0$ denotes the base frame, $\sum_1^a, \sum_1^b$ denote the first joint frames of the two arms, $\sum_e^a, \sum_e^b$ denote the frames of the end-effectors of the two arms, and $\sum_{obj}$ denotes the frame of the object, which located in the center of the mass of the object. $\mathbf{P}_a, \mathbf{P}_b, \mathbf{P}_c \in \mathbb{R}^3$ denote the position vectors of the origins of the frame $\sum_e^a, \sum_e^b, \sum_{obj}$ in the base frame $\sum_0$, respectively. $\mathbf{r}_a, \mathbf{r}_b \in \mathbb{R}^3$ denote the position vectors of the origin of the frame $\sum_{obj}$ in the frame $\sum_e^a, \sum_e^b$, respectively. $\mathbf{g} = -9.8\mathrm{m/s}^2$ is the gravity acceleration.

Before giving the kinematics and dynamics, the following necessary assumptions are made as:

1. The end-effectors of the two arms can grasp the object rigidly, their positions and orientations do not change relatively to the local coordinate of the object (Walker et al., 1991).
2. The forces and moments between the object with the environment and with end-effectors can be measured from the force sensors.

2.1. Kinematics

Based on the position relationships reflected in Figure 1, the following two equations are obtained

$$\mathbf{P}_a = \mathbf{P}_c + {}^0\mathbf{R}_{obj}\mathbf{r}_a \tag{1}$$

$$\mathbf{P}_b = \mathbf{P}_c + {}^0\mathbf{R}_{obj}\mathbf{r}_b \tag{2}$$

where ${}^0\mathbf{R}_{obj} \in \mathbb{R}^{3\times3}$ is the rotation matrix.

Differentiating equations (1) and (2) once, as follows

$$\dot{\mathbf{P}}_a = \dot{\mathbf{P}}_c + \boldsymbol{\omega}_{obj} \times \left({}^0\mathbf{R}_{obj}\mathbf{r}_a\right) = \dot{\mathbf{P}}_c - \mathbf{S}\left({}^0\mathbf{R}_{obj}\mathbf{r}_a\right)\boldsymbol{\omega}_{obj} \tag{3}$$

$$\dot{\mathbf{P}}_b = \dot{\mathbf{P}}_c + \boldsymbol{\omega}_{obj} \times \left({}^0\mathbf{R}_{obj}\mathbf{r}_b\right) = \dot{\mathbf{P}}_c - \mathbf{S}\left({}^0\mathbf{R}_{obj}\mathbf{r}_b\right)\boldsymbol{\omega}_{obj} \tag{4}$$

where $\boldsymbol{\omega}_{obj} \in \mathbb{R}^3$ denote the angle velocity of the object. $\mathbf{S}(\cdot)$ is the skew symmetric matrix of the vector $(\cdot)$.

Because of the angle velocities of any points in one common object are the same, then based on equations (3) and (4), the general velocity relationships are obtained as follows

$$\mathbf{J}_a\dot{\mathbf{q}}_a = \mathbf{J}_{o,a}\dot{\mathbf{X}}_o \tag{5}$$

$$\mathbf{J}_b\dot{\mathbf{q}}_b = \mathbf{J}_{o,b}\dot{\mathbf{X}}_o \tag{6}$$

where $\mathbf{J}_a, \mathbf{J}_b \in \mathbb{R}^{m\times n}(m=6)$ denote the Jacobian matrices of the Arm-a and Arm-b. $\mathbf{q}_a, \mathbf{q}_b \in \mathbb{R}^n$ denote the general joint position vectors of the two arms. $\dot{\mathbf{X}}_o \in \mathbb{R}^m$ is the general velocity of the object. $\mathbf{J}_{o,a}, \mathbf{J}_{o,b} \in \mathbb{R}^{m\times m}$ are the Jacobian matrices defined as follows

$$\mathbf{J}_{o,a} = \begin{bmatrix} \mathbf{I}_3 & -\mathbf{S}\left({}^0\mathbf{R}_{obj}\mathbf{r}_a\right) \\ \mathbf{O}_3 & \mathbf{I}_3 \end{bmatrix} \tag{7}$$

$$\mathbf{J}_{o,b} = \begin{bmatrix} \mathbf{I}_3 & -\mathbf{S}\left({}^0\mathbf{R}_{obj}\mathbf{r}_b\right) \\ \mathbf{O}_3 & \mathbf{I}_3 \end{bmatrix} \tag{8}$$

For convenience, a combined equation is given as

$$\mathbf{J}\dot{\mathbf{q}} = \mathbf{J}_o\dot{\mathbf{X}}_o \tag{9}$$

where $\mathbf{J} = diag[\mathbf{J}_a\ \mathbf{J}_b] \in \mathbb{R}^{2m\times2n}$, $\mathbf{J}_o = [\mathbf{J}_{o,a}^{\mathrm{T}}\ \mathbf{J}_{o,b}^{\mathrm{T}}]^{\mathrm{T}} \in \mathbb{R}^{2m\times m}$ $\mathbf{q} = [\mathbf{q}_a^{\mathrm{T}}\ \mathbf{q}_b^{\mathrm{T}}]^{\mathrm{T}} \in \mathbb{R}^{2n}$.

2.2. Dynamics

The dynamics equations of the two arms can be expressed as follows

$$\begin{aligned}\mathbf{M}(\mathbf{q})\ddot{\mathbf{q}} + \mathbf{C}(\mathbf{q},\dot{\mathbf{q}})\dot{\mathbf{q}} + \mathbf{G}(\mathbf{q}) + \mathbf{K}_c\mathrm{sgn}(\dot{\mathbf{q}}) \\ +\mathbf{K}_v\dot{\mathbf{q}} = \boldsymbol{\tau}_m - \mathbf{J}^T\mathbf{F}\end{aligned} \tag{10}$$

where $\boldsymbol{\tau}_m = [\boldsymbol{\tau}_{m,a}^T\ \boldsymbol{\tau}_{m,b}^T]^T \in \mathbb{R}^{2n}$ denote the torques of the motors after the reducers. $\mathbf{M} = diag(\mathbf{M}_a\ \mathbf{M}_b) \in \mathbb{R}^{2n\times2n}$ is the inertia matrix, $\mathbf{C} = diag(\mathbf{C}_a\ \mathbf{C}_b) \in \mathbb{R}^{2n\times2n}$ are the Coriolis and centrifugal force matrices, $\mathbf{G} = [\mathbf{G}_a^T\ \mathbf{G}_b^T] \in \mathbb{R}^{2n}$ denotes the gravity vector, and $\mathbf{F} = [\mathbf{F}_a^{eT}\ \mathbf{F}_b^{eT}]^T \in \mathbb{R}^{2m}$ is the general force measured from the force sensors located at the end-effectors. $\mathbf{K}_c = diag(\mathbf{K}_{c,a}\ \mathbf{K}_{c,b}) \in \mathbb{R}^{2n\times2n}$ is a diagonal matrix of the Coulomb friction coefficients. $\mathrm{sgn}(\cdot)$ denotes the signal function. $\mathbf{K}_v = diag(\mathbf{K}_{v,a}\ \mathbf{K}_{v,b}) \in \mathbb{R}^{2n\times2n}$ is a diagonal matrix of the viscous friction coefficients.

In fact, the control scheme designed in the next section is based on the recursive dynamics, so that the above dynamics will not be used in the design of the controller. The dynamics of each general link can be expressed by the Newton–Euler formulation as follows (Zhu, 2010)

$${}^i\mathbf{M}_i \cdot {}^i\tilde{\mathbf{V}}_i + {}^i\mathbf{C}_i \cdot {}^i\mathbf{V}_i + {}^i\mathbf{G}_i = {}^i\mathbf{F}_i^* \tag{11}$$

where ${}^i\mathbf{M}_i \in \mathbb{R}^{6\times6}$, ${}^i\mathbf{C}_i \in \mathbb{R}^{6\times6}$, and ${}^i\mathbf{G}_i \in \mathbb{R}^6$ represent the mass matrix, Coriolis and centrifugal force matrices, and the

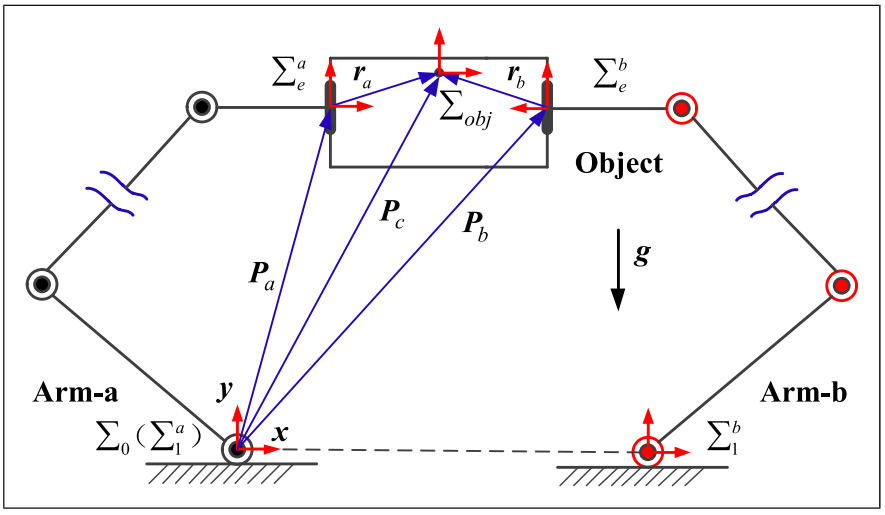

Figure 1. Dual-arm system and the position relationship.

gravity vector of ith link expressed in the ith link frame. ${}^i\mathbf{F}_i^* \in \mathbb{R}^6$ is the total net forces and moments acting on the link. ${}^i\mathbf{V}_i \in \mathbb{R}^6$ is the general velocity of the link. ${}^i\tilde{\mathbf{V}}_i = \frac{d}{dt}({}^i\mathbf{V}_i)$ is the general acceleration. The definition of them can be found in (Zhu, 2010).

The dynamics of each joint can be directly presented as

$$B_i\ddot{q}_i + K_{c,i}sgn(\dot{q}_i) + K_{v,i}\dot{q}_i + c_i = \tau_i^* \tag{12}$$

where $B_i \in \mathbb{R}$ denotes the moment of inertia of the ith joint, $K_{c,i}, K_{v,i} \in \mathbb{R}$ denote the ith element of the $\mathbf{K}_c, \mathbf{K}_v$, respectively. $c_i \in \mathbb{R}$ denotes an offset that accommodates asymmetric Coulomb frictions. $\tau_i^* \in \mathbb{R}$ denotes the net torque devoted to the joint dynamics (Zhu, 2010).

To design the recursive adaptive control algorithm, equation (11) needs to be linearization, as follows

$${}^i\mathbf{F}_i^* = {}^i\mathbf{Y}_i\left({}^i\mathbf{V}_i, {}^i\tilde{\mathbf{V}}_i\right){}^i\mathbf{\Theta}_i \tag{13}$$

where ${}^i\mathbf{Y}_i \in \mathbb{R}^{6\times 13}$ is the regressor matrix, and ${}^i\mathbf{\Theta}_i \in \mathbb{R}^{13\times 1}$ is the vector of the dynamics parameters.

Equation (12) also needs to be linearization yields

$$\tau_i^* = \mathbf{Y}_i^{\text{joint}}\mathbf{\Theta}_i^{\text{joint}} \tag{14}$$

where $\mathbf{Y}_i^{\text{joint}} = [\ddot{q}_i \ sgn(\dot{q}_i) \ \dot{q}_i \ 1]$, $\mathbf{\Theta}_i^{\text{joint}} = [B_i \ k_{c,i} \ k_{v,i} \ c_i]^T$.

Similar to equation (11), the dynamics of the object can be obtained used the Newton–Euler formulation as

$$\mathbf{M}_o(\mathbf{X}_o)\ddot{\mathbf{X}}_o + \mathbf{C}_o(\mathbf{X}_o, \dot{\mathbf{X}}_o)\dot{\mathbf{X}}_o + \mathbf{G}_o(\mathbf{X}_o) = \mathbf{J}_o^T\mathbf{F} \tag{15}$$

where $\mathbf{M}_o \in \mathbb{R}^{m\times m}$, $\mathbf{C}_o \in \mathbb{R}^{m\times m}$, and $\mathbf{G}_o \in \mathbb{R}^m$ denote the mass matrix, Coriolis and centrifugal matrices, and the gravity vector of the object expressed in the base frame.

Based on equation (15), the inverse solution of the general force $\mathbf{F}$ can be resolved as (Lin and Goldenberg, 1997)

$$\mathbf{F} = \left(\mathbf{J}_o^T\right)^\dagger\left[\mathbf{M}_o\ddot{\mathbf{X}}_o + \mathbf{C}_o\dot{\mathbf{X}}_o + \mathbf{G}_o\right] + \mathbf{F}_I \tag{16}$$

where $\left(\mathbf{J}_o^T\right)^\dagger$ is the pseudo-inverse matrix of the $\mathbf{J}_o^T$, $\mathbf{F}_I \in \mathbb{R}^{2m}$ is the internal force which does not contribute to the motion of the object, due to this, it is located in the null space of the $\mathbf{J}_o^T$. It is assumed that $\mathbf{F}$ can be measured from the force sensors, so that it can be divided by the external forces $\mathbf{F}_E$ and internal forces $\mathbf{F}_I$ as follows

$$\mathbf{F} = \mathbf{F}_E + \mathbf{F}_I \tag{17}$$

$$\mathbf{F}_E = \left(\mathbf{J}_o^T\right)^\dagger\mathbf{J}_o^T\mathbf{F} \tag{18}$$

$$\mathbf{F}_I = \left[\mathbf{I}_{12} - \left(\mathbf{J}_o^T\right)^\dagger\mathbf{J}_o^T\right]\mathbf{F} \tag{19}$$

where $[\mathbf{I}_{12} - (\mathbf{J}_o^T)^\dagger\mathbf{J}_o^T]$ is the null-space matrix of $\mathbf{J}_o^T$.

3. Dual-loop control scheme

In this section, the dual-loop adaptive variable impedance control scheme is presented, which includes three main parts, as the following description.

3.1. Low-level VDC control scheme

The virtual decomposition control (VDC) is a position control scheme which is used to replace the servo control scheme that is used in most of the dual-arm system. And the recursive process of the VDC includes the kinematics forward recursion and dynamics backward recursion, as:

VDC

1: Input: $\mathbf{q}_{r,k}\ \ \dot{\mathbf{q}}_{r,k}\ \ \ddot{\mathbf{q}}_{r,k}, \mathbf{q}_k\ \ \dot{\mathbf{q}}_k$
2: Output: $\tau_{k,i}^{\text{link}}$
3: Initialize: ${}^0\mathbf{V}_0\ \ {}^0\tilde{\mathbf{V}}_0 = \mathbf{O}_{6\times1}, {}^{n+1}\mathbf{F}_{n+1,r} = \mathbf{O}_{6\times1}$
4: For $i = 1:n$ Forward Recursion
5: ${}^i\mathbf{V}_i = {}^i\mathbf{T}_{i-1}\,{}^{i-1}\mathbf{V}_{i-1} + \mathbf{e}_{z6}\dot{q}_{k,i}$
6: ${}^i\mathbf{V}_{i,r} = {}^i\mathbf{T}_{i-1}\,{}^{i-1}\mathbf{V}_{i-1,r} + \mathbf{e}_{z6}\dot{q}_{r,k,i}$
7: ${}^i\tilde{\mathbf{V}}_{i,r} = {}^i\dot{\mathbf{T}}_{i-1}\,{}^{i-1}\mathbf{V}_{i-1,r} + {}^i\mathbf{T}_{i-1}\,{}^{i-1}\tilde{\mathbf{V}}_{i-1,r} + \mathbf{e}_{z6}\ddot{q}_{r,k,i}$
8: End
9: For $i = n:1$ Backward Recursion
10:
${}^i\mathbf{F}_{i,r}^* = \mathbf{Y}_{i,r}({}^i\mathbf{V}_i, {}^i\mathbf{V}_{i,r}, {}^i\tilde{\mathbf{V}}_{i,r})\,{}^i\hat{\boldsymbol{\theta}}_i + \mathbf{K}_{Di}({}^i\mathbf{V}_{i,r} - {}^i\mathbf{V}_i)$
11: ${}^i\dot{\hat{\boldsymbol{\theta}}}_i = \mathbf{P}_i\mathbf{Y}_{i,r}^T({}^i\mathbf{V}_{i,r} - {}^i\mathbf{V}_i)$
12: ${}^i\mathbf{F}_{i,r} = {}^{i+1}\mathbf{T}_i^T\,{}^{i+1}\mathbf{F}_{i+1,r} + {}^i\mathbf{F}_{i,r}^*$
13: $\tau_{k,i}^{\text{link}} = \mathbf{e}_{z6}^T\,{}^i\mathbf{F}_{i,r}$
14: End

where $\mathbf{q}_{r,k} \in \mathbb{R}^n$ is the reference position which will be computed in the next part. The subscript $k = a$ or b denote the choice of Arm-a or Arm-b. $\mathbf{e}_{z6} = [0\ 0\ 0\ 0\ 0\ 1]^T$, ${}^i\mathbf{T}_{i-1}$ is the general velocity transformation matrix. $\mathbf{K}_{Di} \in \mathbb{R}^{m\times m}$ is the control gain, which is usually is a positive definite diagonal matrix, $\mathbf{P}_i \in \mathbb{R}^{13\times13}$ is the parameters update gain, which is a positive definite diagonal matrix. ${}^i\widehat{\boldsymbol{\theta}}_i$ are the estimated dynamics parameters.

The pseudo code above contains only the link dynamics control, the joint dynamics control can be resolved as the following equation, based on equation (14), yields

$$\tau_{k,i}^* = \mathbf{Y}_{r,i}^{\text{joint}}\widehat{\boldsymbol{\Theta}}_i^{\text{joint}} + k_{d,i}(\dot{q}_{r,k,i} - \dot{q}_{k,i}) \tag{20}$$

$$\dot{\widehat{\boldsymbol{\Theta}}}_i^{\text{joint}} = P_i^{\text{joint}}\left(\mathbf{Y}_{r,i}^{\text{joint}}\right)^T(\dot{q}_{r,k,i} - \dot{q}_{k,i}) \tag{21}$$

where $k_{d,i} \in \mathbb{R}$ and $P_i^{\text{joint}} \in \mathbb{R}$ are the positive gains.

Then the final torques of the motors are obtained as

$$\tau_{k,i}^{\text{motor}} = \tau_{k,i}^* + \tau_{k,i}^{\text{link}} \tag{22}$$

3.2. Inner-loop impedance control scheme based on the internal force

To obtain the desired internal force tracking, an impedance control scheme based on the internal force is designed in this part, as follows

$$\mathrm{H}_d\Delta\ddot{\mathbf{X}}_e + \mathbf{D}_d\Delta\dot{\mathbf{X}}_e + \mathbf{K}_d\Delta\mathbf{X}_e = \mathbf{F}_I - \mathbf{F}_{I,d} \tag{23}$$

where $\Delta\mathbf{X}_e \in \mathbb{R}^{2m}$ is the general position deviation of the end-effectors. $\mathrm{H}_d, \mathbf{D}_d, \mathbf{K}_d$ are the desired mass matrix, damping matrix, and stiffness matrix, respectively, as follows

$$\mathbf{H}_d = diag(\mathbf{H}_{d,a}, \mathbf{H}_{d,b}) \in \mathbb{R}^{2m\times2m}$$

$$\mathbf{D}_d = diag(\mathbf{D}_{d,a}, \mathbf{D}_{d,b}) \in \mathbb{R}^{2m\times2m}$$

$$\mathbf{K}_d = diag(\mathbf{K}_{d,a}, \mathbf{K}_{d,b}) \in \mathbb{R}^{2m\times2m}$$

Remark 1. the expressions of the deviation of the rotational and translational directions are different in the form, we use the $\Delta\mathbf{X}_e$ denotes all the directions, the readers can refer to the detailed expressions in the (Heck et al., 2013).

Based on equation (23), the reference acceleration of the end-effectors which is used in the VDC control scheme can be resolved as follows

$$\ddot{\mathbf{X}}_{e,r} = \ddot{\mathbf{X}}_{e,d} - \mathrm{H}_d^{-1}\left[\mathbf{D}_d\Delta\dot{\mathbf{X}}_e + \mathbf{K}_d\Delta\mathbf{X}_e + (\mathbf{F}_I - \mathbf{F}_{I,d})\right] \tag{24}$$

Integral equation (24), the reference velocity is obtained

$$\dot{\mathbf{X}}_{e,r} = \dot{\mathbf{X}}_{e,d} - \int_0^t\left\{\mathrm{H}_d^{-1}\left[\mathbf{D}_d\Delta\dot{\mathbf{X}}_e + \mathbf{K}_d\Delta\mathbf{X}_e + (\mathbf{F}_I - \mathbf{F}_{I,d})\right]\right\}dt \tag{25}$$

The joint reference velocity and acceleration used in the VDC are obtained as follows

$$\dot{\mathbf{q}}_r = \mathbf{J}^{-1}(\mathbf{q})\dot{\mathbf{X}}_{e,r} \tag{26}$$

$$\ddot{\mathbf{q}}_r = \mathbf{J}^{-1}(\mathbf{q})\left[\ddot{\mathbf{X}}_{e,r} - \mathbf{J}(\mathbf{q})\dot{\mathbf{q}}\right] \tag{27}$$

Note that the desired position, velocity, and acceleration $\mathbf{X}_{e,d}, \dot{\mathbf{X}}_{e,d}, \ddot{\mathbf{X}}_{e,d}$ will be modified by the outer-loop variable impedance control in the Part C.

Moreover, to enhance the internal force tracking performance, a direct internal force control is designed in the proposed scheme, as follows

$$\boldsymbol{\tau}_F = \mathbf{J}^T\left[\mathbf{F}_{I,d} + \mathbf{K}_{Ip}(\mathbf{F}_{I,d} - \mathbf{F}_I) + \mathbf{K}_{Ii}\int_0^t(\mathbf{F}_{I,d} - \mathbf{F}_I)dt\right] \tag{28}$$

where $\mathbf{K}_{Ip}, \mathbf{K}_{Ii} \in \mathbb{R}^{2m\times2m}$ are the proportional and integral gains, which are usually set as diagonal matrices.

3.3. Outer-loop adaptive impedance control scheme

The interaction of the object with the environment is challenging due to the unknown stiffness and position of the environment. In the Part C, the adaptive variable impedance control method is designed.

Firstly, the non-adaptive impedance control formulation is given as follows

$$\mathrm{H}_o\Delta\ddot{\mathbf{X}}_o + \mathbf{D}_o\Delta\dot{\mathbf{X}}_o + \mathbf{K}_o\Delta\mathbf{X}_o = \mathbf{F}_{env} - \mathbf{F}_{env,d} \tag{29}$$

where $\Delta\mathbf{X}_o \in \mathbb{R}^m$ is the general position deviation of the object, $\mathrm{H}_d, \mathbf{D}_d, \mathbf{K}_d \in \mathbb{R}^{m\times m}$ are the desired mass, damping, and stiffness matrix of the object, respectively. $\mathbf{F}_{env} \in \mathbb{R}^m$ is the general force acted on the object by the environment, $\mathbf{F}_{env,d} \in \mathbb{R}^m$ is the desired general force.

For convenience, only one translation direction is considered in this paper, and the adaptive variable impedance control is designed as follows (Song et al., 2021; Hu and Cao, 2022; Jinjun et al., 2019; Roveda and Piga, 2020)

$$H_o\Delta\ddot{\widehat{X}}_o + D_o(t)\Delta\dot{\widehat{X}}_o + K_o\left[\Delta\widehat{X}_o + \psi(t)\right] = F_{env} - F_{env,d} \tag{30}$$

$$\psi(t) = \psi(t-\Delta t) + \alpha\frac{F_{env,d}(t-\Delta t) - F_{env}(t-\Delta t)}{K_o} \tag{31}$$

$$d(t) = d_0 - (d_0 - 1)e^{-\beta|F_{env}(t) - F_{env}(t-\Delta t)|} \tag{32}$$

$$D_o(t) = 2d(t)\sqrt{K_o H_o} \tag{33}$$

where $\Delta\widehat{X}_o = \Delta X_o + \delta X_o$, $\alpha \in \mathbb{R}^+$ is the update gain, which is a positive constant, $d_0, \beta \in \mathbb{R}^+$ are positive constants, Δt is the sampling time.

To understand the overall control scheme, the control flow chart can be illustrated as shown in Figure 2:where the deviations $\Delta\widehat{X}_o, \Delta\dot{\widehat{X}}_o, \Delta\ddot{\widehat{X}}_o$ will be resolved in the block "Outer-loop Impedance control" according with the dynamic damping $D_o(t)$ and position $\psi(t)$ in the "Adaptive" block, and then the deviations $\Delta X_{e,d}, \Delta\dot{X}_{e,d}, \Delta\ddot{X}_{e,d}$ of the two end-effectors can be obtained. Note that the above deviations correspond to one translation direction, and the other directions will not be considered in this paper. The reference trajectory in the Cartesian space can be resolved in the "Inter-loop Impedance control" block, then the reference trajectory in the joint space can be obtained from the "Inverse Kinematics" block. Based on the resolved reference trajectory in the joint space, the required torques can be resolved by the "VDC" block, where the joint dynamics control in equations (20) and (21) is neglected in the schema. The direct internal force control can be resolved in the "Internal force control" block, before that the internal force needs to be separated in the "Separate internal force" block. Through the "Forward Kinematics" block, the real-time position of the end-effectors can be obtained, where, the joint positions can be read from the joint position sensors.

4. Stability analysis

4.1. The VDC stability analysis

The stability of the low-level position control is firstly given. Define the Lyapunov-like function as follows (Wang, 2021; Li et al., 2021)

$$\mathrm{V} = \sum_{i=1}^{n}\mathrm{V}_i \tag{34}$$

$$\mathrm{V}_i = \frac{1}{2}\left({}^i\mathbf{V}_{i,r} - {}^i\mathbf{V}_i\right)^T {}^i\mathbf{M}_i\left({}^i\mathbf{V}_{i,r} - {}^i\mathbf{V}_i\right) + \frac{1}{2}{}^i\tilde{\boldsymbol{\theta}}_i^T\mathbf{P}_i^{-1}{}^i\tilde{\boldsymbol{\theta}}_i \tag{35}$$

where ${}^i\tilde{\boldsymbol{\theta}}_i = {}^i\widehat{\boldsymbol{\theta}}_i - {}^i\boldsymbol{\theta}_i$.

Differentiating equation (35) with respect to time as follows

$$\dot{\mathrm{V}}_i = \left({}^i\mathbf{V}_{i,r} - {}^i\mathbf{V}_i\right)^T {}^i\mathbf{M}_i\left({}^i\dot{\tilde{\mathbf{V}}}_{i,r} - {}^i\dot{\tilde{\mathbf{V}}}_i\right) + \tilde{\boldsymbol{\theta}}_i^T\mathbf{P}_i^{-1}\dot{\tilde{\boldsymbol{\theta}}}_i \tag{36}$$

Based on equation (11) and the $10-$th equation in the VDC algorithm, the following two equations are obtained

$${}^i\mathbf{M}_i{}^i\dot{\tilde{\mathbf{V}}}_i = {}^i\mathbf{F}_i^* - {}^i\mathbf{C}_i\cdot{}^i\mathbf{V}_i - {}^i\mathbf{G}_i \tag{37}$$

$$\begin{aligned}{}^i\mathbf{M}_i{}^i\dot{\tilde{\mathbf{V}}}_{i,r} = {}^i\mathbf{F}_{i,r}^* - {}^i\tilde{\mathbf{M}}_i\cdot{}^i\dot{\tilde{\mathbf{V}}}_{i,r} - \left({}^i\tilde{\mathbf{C}}_i + {}^i\mathbf{C}_i\right)\cdot{}^i\mathbf{V}_{i,r}\\ - \left({}^i\tilde{\mathbf{G}}_i + {}^i\mathbf{G}_i\right) - \mathbf{K}_{Di}\left({}^i\mathbf{V}_{i,r} - {}^i\mathbf{V}_i\right)\end{aligned} \tag{38}$$

where ${}^i\tilde{\mathbf{M}}_i = {}^i\widehat{\mathbf{M}}_i - {}^i\mathbf{M}_i$, ${}^i\tilde{\mathbf{C}}_i = {}^i\widehat{\mathbf{C}}_i - {}^i\mathbf{C}_i$ ${}^i\tilde{\mathbf{G}}_i = {}^i\widehat{\mathbf{G}}_i - {}^i\mathbf{G}_i$

Substituting equations (38) and (37) into (36) yields

$$\begin{aligned}\dot{\mathrm{V}}_i = &-\left({}^i\mathbf{V}_{i,r} - {}^i\mathbf{V}_i\right)^T\mathbf{K}_{D,i}\left({}^i\mathbf{V}_{i,r} - {}^i\mathbf{V}_i\right)\\ &+\left({}^i\mathbf{V}_{i,r} - {}^i\mathbf{V}_i\right)^T\left({}^i\mathbf{F}_{i,r}^* - {}^i\mathbf{F}_i^*\right) + \tilde{\boldsymbol{\theta}}_i^T\mathbf{P}_i^{-1}\dot{\tilde{\boldsymbol{\theta}}}_i\\ &-\left({}^i\mathbf{V}_{i,r} - {}^i\mathbf{V}_i\right)^T\mathbf{Y}_{i,r}\tilde{\boldsymbol{\theta}}_i - \left({}^i\mathbf{V}_{i,r} - {}^i\mathbf{V}_i\right)^T{}^i\mathbf{C}_i\left({}^i\mathbf{V}_{i,r} - {}^i\mathbf{V}_i\right)\end{aligned} \tag{39}$$

Substituting the $11-$th equation in the VDC into (39), and ${}^i\mathbf{C}_i$ being skew-symmetric yields

$$\begin{aligned}\dot{\mathrm{V}}_i = &-\left({}^i\mathbf{V}_{i,r} - {}^i\mathbf{V}_i\right)^T\mathbf{K}_{D,i}\left({}^i\mathbf{V}_{i,r} - {}^i\mathbf{V}_i\right)\\ &+\left({}^i\mathbf{V}_{i,r} - {}^i\mathbf{V}_i\right)^T\left({}^i\mathbf{F}_{i,r}^* - {}^i\mathbf{F}_i^*\right)\end{aligned} \tag{40}$$

The sum of $\dot{\mathrm{V}}_i$ yields

$$\begin{aligned}\dot{\mathrm{V}} = \sum_{i=1}^{n}\dot{\mathrm{V}}_i = &-\sum_{i=1}^{n}\left({}^i\mathbf{V}_{i,r} - {}^i\mathbf{V}_i\right)^T\mathbf{K}_{D,i}\left({}^i\mathbf{V}_{i,r} - {}^i\mathbf{V}_i\right)\\ &+\sum_{i=1}^{n}\left({}^i\mathbf{V}_{i,r} - {}^i\mathbf{V}_i\right)^T\left({}^i\mathbf{F}_{i,r}^* - {}^i\mathbf{F}_i^*\right)\end{aligned} \tag{41}$$

Due to the following recursion form

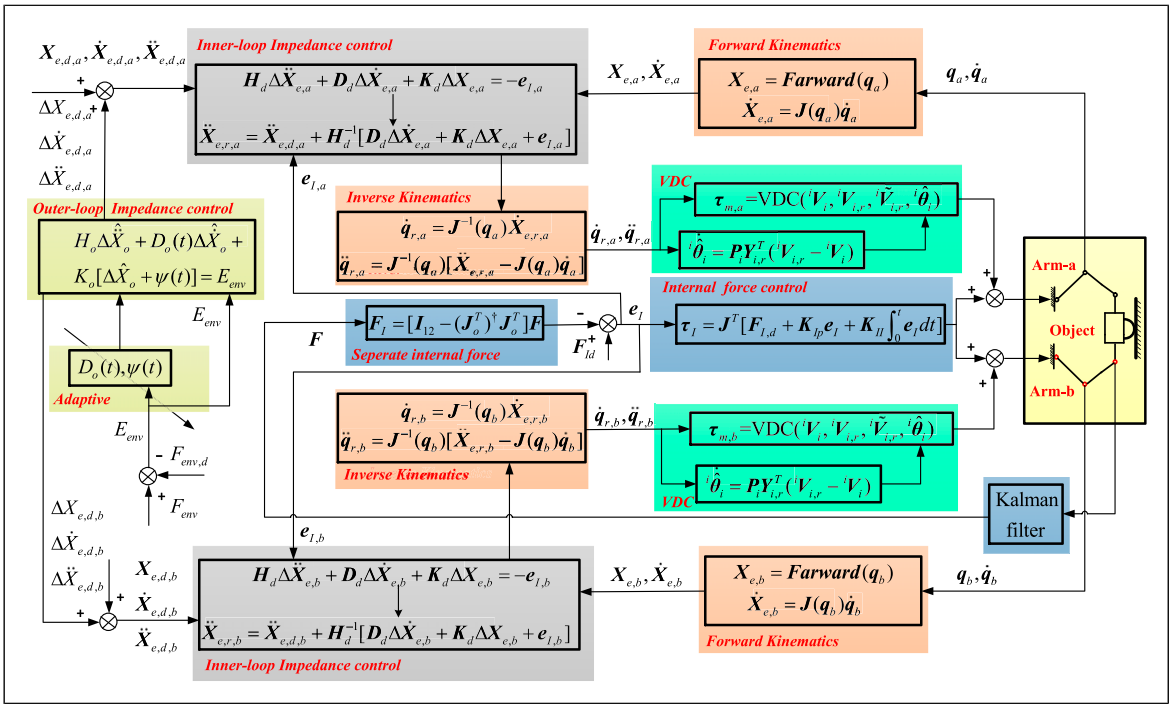

Figure 2. Dual-loop impedance control schema.

$$\begin{aligned}&\sum_{i=1}^{n}\left({}^{i}\mathbf{V}_{i,r}-{}^{i}\mathbf{V}_{i}\right)^{T}\left({}^{i}\mathbf{F}_{i,r}^{*}-{}^{i}\mathbf{F}_{i}^{*}\right)=\\&\left({}^{0}\mathbf{V}_{0,r}-{}^{0}\mathbf{V}_{0}\right)^{T}\left({}^{0}\mathbf{F}_{0,r}-{}^{0}\mathbf{F}_{0}\right)-\left({}^{1}\mathbf{V}_{1,r}-{}^{1}\mathbf{V}_{1}\right)^{T}\left({}^{1}\mathbf{F}_{1,r}-{}^{1}\mathbf{F}_{1}\right)+\\&\left({}^{1}\mathbf{V}_{1,r}-{}^{1}\mathbf{V}_{1}\right)^{T}\left({}^{1}\mathbf{F}_{1,r}-{}^{1}\mathbf{F}_{1}\right)-\left({}^{2}\mathbf{V}_{2,r}-{}^{2}\mathbf{V}_{2}\right)^{T}\left({}^{2}\mathbf{F}_{2,r}-{}^{2}\mathbf{F}_{2}\right)+\\&\vdots\\&+\left({}^{n}\mathbf{V}_{n,r}-{}^{n}\mathbf{V}_{n}\right)^{T}\left({}^{n}\mathbf{F}_{n,r}-{}^{n}\mathbf{F}_{n}\right)\\&-\left({}^{n\,1}\mathbf{V}_{n+1,r}-{}^{n\,1}\mathbf{V}_{n+1}\right)^{T}\left({}^{n\,1}\mathbf{F}_{n+1,r}-{}^{n\,1}\mathbf{F}_{n+1}\right)\\&=\left({}^{0}\mathbf{V}_{0,r}-{}^{0}\mathbf{V}_{0}\right)^{T}\left({}^{0}\mathbf{F}_{0,r}-{}^{0}\mathbf{F}_{0}\right)\\&-\left({}^{n\,1}\mathbf{V}_{n+1,r}-{}^{n\,1}\mathbf{V}_{n+1}\right)^{T}\left({}^{n\,1}\mathbf{F}_{n+1,r}-{}^{n\,1}\mathbf{F}_{n+1}\right)=0\end{aligned}\tag{42}$$

So that, we obtain the final derivation of the Lyapunov-like function

$$\dot{\mathrm{V}}=-\sum_{i=1}^{n}\left({}^{i}\mathbf{V}_{i,r}-{}^{i}\mathbf{V}_{i}\right)^{T}\mathbf{K}_{D,i}\left({}^{i}\mathbf{V}_{i,r}-{}^{i}\mathbf{V}_{i}\right)\leq 0\tag{43}$$

The system trajectories are thus guaranteed to reach the reference trajectories, and the reference trajectories will be resolved from the inner-loop impedance control scheme, which is a cascaded structure.

4.2. The inner-loop stability analysis

Define the following Lyapunov function as follows (Bonitz and Hsia, 1996a)

$$\mathrm{V}_{inner-loop}=\frac{1}{2}\Delta\dot{\mathbf{X}}_{e}^{T}\mathrm{H}_{d}\Delta\dot{\mathbf{X}}_{e}+\frac{1}{2}\Delta\mathbf{X}_{e}^{T}\mathbf{K}_{d}\Delta\mathbf{X}_{e}\tag{44}$$

Differentiating equation (44) yields

$$\dot{\mathrm{V}}_{inner-loop}=\Delta\dot{\mathbf{X}}_{e}^{T}\left(\mathrm{H}_{d}\Delta\ddot{\mathbf{X}}_{e}+\mathbf{K}_{d}\Delta\mathbf{X}_{e}\right)\tag{45}$$

Substituting $\mathrm{H}_{d}\Delta\ddot{\mathbf{X}}_{e}+\mathbf{K}_{d}\Delta\mathbf{X}_{e}=\mathbf{F}_{I}-\mathbf{F}_{I,d}-\mathbf{D}_{d}\Delta\dot{\mathbf{X}}_{e}$ into equation (45) yields

$$\dot{\mathrm{V}}_{inner-loop}=\Delta\dot{\mathbf{X}}_{e}^{T}\left(\mathbf{F}_{I}-\mathbf{F}_{I,d}\right)-\Delta\dot{\mathbf{X}}_{e}^{T}\mathbf{D}_{d}\Delta\dot{\mathbf{X}}_{e}\tag{46}$$

Due to $(\mathbf{F}_{I}-\mathbf{F}_{I,d})$ locates in the null-space of $\mathbf{J}_{o}^{T}$, so that

$$\dot{\mathrm{V}}_{inner-loop}=-\Delta\dot{\mathbf{X}}_{e}^{T}\mathbf{D}_{d}\Delta\dot{\mathbf{X}}_{e}\leq 0\tag{47}$$

If a variable impedance control is used in the internal force control, equation (47) will be modified as follows

$$\dot{\mathrm{V}}_{inner-loop}=-\Delta\dot{\mathbf{X}}_{e}^{T}\mathbf{D}_{d}(t)\Delta\dot{\mathbf{X}}_{e}+\frac{1}{2}\Delta\mathbf{X}_{e}^{T}\dot{\mathbf{K}}_{d}(t)\Delta\mathbf{X}_{e}\tag{48}$$

Observing from equation (48), the variable stiffness $\dot{\mathbf{K}}_{d}(t)$ will not guarantee $\dot{\mathrm{V}}_{inner-loop}\leq 0$, in other words, the variation of the stiffness produces extra energy that is injected into the system destroying its passivity, although there are some methods to resolve this problem, however, to guarantee a steady grasp, the impedance parameters in the internal force control will be fixed in this paper(Ferraguti et al., 2013).

The close-loop dynamics of the direct internal force control in equation (28) can be obtained as

$$\left(\mathbf{K}_{Ip}+1\right)\left(\mathbf{F}_{I,d}-\mathbf{F}\right)+\mathbf{K}_{Ii}\int_0^t\left(\mathbf{F}_{I,d}-\mathbf{F}\right)dt=\mathbf{O}_{2m\times 2m} \tag{49}$$

Because of equation (49) being linear, the internal force control can obtain an exponential convergence speed, which is important for the dual-arm manipulator coordinately grasp the object steadily.

4.3. The outer-loop stability analysis

To illustrate the outer-loop stability, the model of the environment needs to be considered as follows (Erickson et al., 2003)

$$K_{env}(X_{env}-X_c)=F_{env} \tag{50}$$

where K_{env} is the stiffness of the environment, X_c is the contact point of the object and the environment. For convenience, it is assumed that $X_o=X_c$.

Substituting equation (31) into equation (30) yields

$$\begin{aligned}&H_o\Delta\ddot{\widehat{X}}_o+D_o(t)\Delta\dot{\widehat{X}}_o+K_o\Delta\widehat{X}_o+K_o\psi(t^-)\\&\quad+\alpha[F_{env,d}(t^-)-F_{env}(t^-)]=F_{env}-F_{env,d}\end{aligned} \tag{51}$$

where $t^-=t-\Delta t$ denotes the last sampling time.

According the following equations

$$\begin{cases}\Delta\widehat{X}_o=\Delta X_o+\delta X_o\\ \Delta\dot{\widehat{X}}_o=\Delta\dot{X}_o+\delta\dot{X}_o\\ \Delta\ddot{\widehat{X}}_o=\Delta\ddot{X}_o+\delta\ddot{X}_o\end{cases} \tag{52}$$

Substituting equation (52) into (51) yields

$$\begin{aligned}&H_o\Delta\ddot{X}_o+D_o(t)\Delta\dot{X}_o+K_o\Delta X_o+K_o\psi(t^-)\\&+\alpha[F_{env,d}(t^-)-F_{env}(t^-)]+(F_{env,d}-F_{env})\\&=-H_o\delta\ddot{X}_e-D_o(t)\delta\dot{X}_e-K_o\delta X_e\end{aligned} \tag{53}$$

According the following equations

$$\begin{cases}\Delta X_o=-F_{env}/K_{env}\\ \Delta\dot{X}_o=-\dot{F}_{env}/K_{env}\\ \Delta\ddot{X}_o=-\ddot{F}_{env}/K_{env}\end{cases} \tag{54}$$

Substituting equation (54) into (53) yields

$$\begin{aligned}&-H_o\ddot{F}_{env}-D_o(t)\dot{F}_{env}-K_oF_{env}+K_{env}K_o\psi(t^-)\\&+K_{env}\alpha[F_{env,d}(t^-)-F_{env}(t^-)]+K_{env}(F_{env,d}-F_{env})\\&=-H_oK_{env}\delta\ddot{X}_e-D_o(t)K_{env}\delta\dot{X}_e-K_oK_{env}\delta X_e\end{aligned} \tag{55}$$

According the following equations

$$\begin{cases}\widehat{F}_{env}=K_{env}\delta X_e\\ \dot{\widehat{F}}_{env}=K_{env}\delta\dot{X}_e\\ \ddot{\widehat{F}}_{env}=K_{env}\delta\ddot{X}_e\end{cases} \tag{56}$$

Substituting equation (56) into (55) yields

$$\begin{aligned}&H_o\ddot{C}(t)+D_o(t)\dot{C}(t)+(K_o+K_{env})C(t)+K_{env}K_o\psi(t^-)\\&+K_{env}\alpha C(t^-)=H_o\ddot{R}(t)+D_o(t)\dot{R}(t)+K_oR(t)\end{aligned} \tag{57}$$

where
$C(t)=F_{env,d}(t)-F_{env}(t), R(t)=F_{env,d}(t)-\widehat{F}_{env}(t)$.

Observing from equation (31) we obtain

$$\begin{cases}K_o\psi(t-\Delta t)-K_o\psi(t-2\Delta t)=\alpha C(t-2\Delta t)\\ K_o\psi(t-2\Delta t)-K_o\psi(t-3\Delta t)=\alpha C(t-3\Delta t)\\ \vdots\\ K_o\psi(t-N\Delta t)-K_o\psi(t-(N+1)\Delta t)=\alpha C(t-(N+1)\Delta t)\end{cases} \tag{58}$$

Setting $\psi(t-(N+1)\Delta t)=0$, and substituting equation (58) into (57) yields

$$\begin{aligned}&H_o\ddot{C}(t)+D_o(t)\dot{C}(t)+(K_o+K_{env})C(t)+\alpha K_{env}\Big[C(t^-)+\\&\cdots+C(t-(N+1)\Delta t)\Big]=H_o\ddot{R}(t)+D_o(t)\dot{R}(t)+K_oR(t)\end{aligned} \tag{59}$$

The Laplace transformation of equation (59) is as follows

$$\frac{C(s)}{R(s)}=\frac{H_os^2+D_o(t)s+K_o}{H_os^2+D_o(t)s+K_o+K_{env}+\alpha K_{env}(e^{-\Delta ts}+\cdots+e^{-(N+1)\Delta ts})} \tag{60}$$

The characteristic equation of equation (60) is as follows

$$H_os^2+D_o(t)s+K_o+K_{env}+\alpha K_{env}\left(e^{-\Delta ts}+\cdots+e^{-(N+1)\Delta ts}\right)=0 \tag{61}$$

If $|e^{-\Delta ts}|\neq 1$, and assume N is enough big, we obtain

$$\sum_n^{\infty}e^{-N\Delta ts}=\frac{1}{1-e^{-\Delta ts}}-1 \tag{62}$$

When the sampling time $0<\Delta t\ll 1$, $1-e^{-\Delta ts}\approx\Delta ts$, substituting equation (62) into (61) yields

$$\Delta tH_os^3+\Delta tD_o(t)s^2+\Delta t[K_o+K_{env}(1-\alpha)K_{env}]s+\alpha K_{env}=0 \tag{63}$$

Based on the Routh criterion, the stability condition needs to satisfy the following inequality

$$0<\alpha<\frac{\Delta tD_o(t)(K_o+K_{env})}{[H_o+\Delta tD_o(t)]K_{env}} \tag{64}$$

From equation (32), we know that $d(t)\geq 1$, so that

$$D_o(t)\geq 2\sqrt{K_oH_o} \tag{65}$$

Substituting equation (65) into (64) yields

$$0<\alpha<\frac{2\Delta t\sqrt{K_oH_o}(K_o+K_{env})}{\left(H_o+2\Delta t\sqrt{K_oH_o}\right)K_{env}} \tag{66}$$

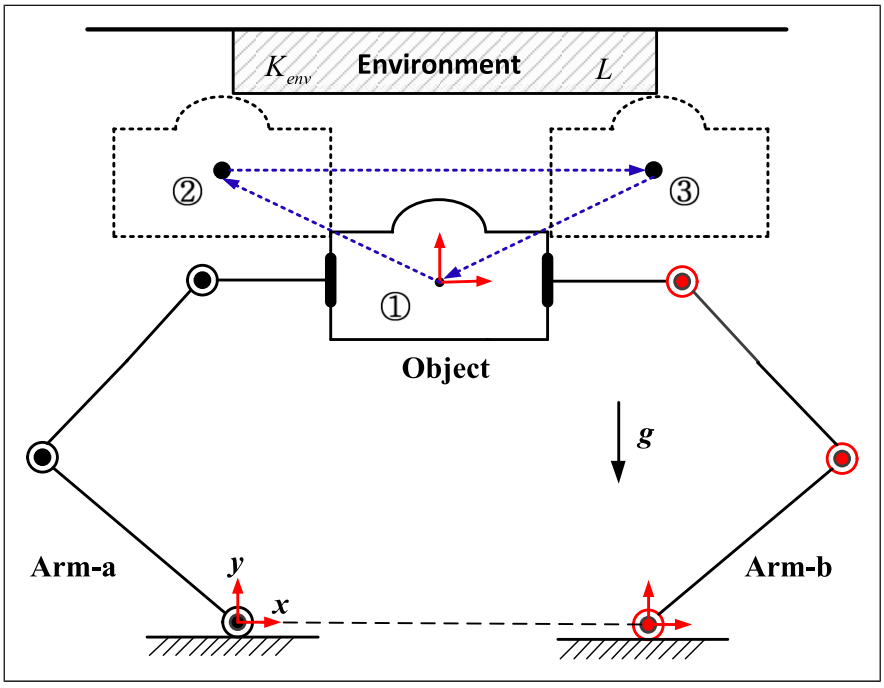

Figure 3. Dual-arm system and the environment.

Table 1. DAUL-ARM system parameters.

Items	Length(m)	Mass(kg)	CoM(m)	Inertia(Kgm^2)
Link1	1	1	0.5	0.02
Link2	1	1	0.5	0.015
Link3	0.25	0.25	0.125	0.005
Object	0.5	3	0.25	0.005

K_{env} is unknown, and $(K_o + K_{env}) > K_{env}$, the more conservative condition is obtained

$$0 < \alpha < \frac{2\Delta t\sqrt{K_o H_o}}{\left(H_o + 2\Delta t\sqrt{K_o H_o}\right)} \tag{67}$$

When the input is a step signal, $R(s) = 1/s$, the steady-state error is as follows

$$\begin{aligned} e_{ss} &= \lim_{t\to\infty} C(t) = \lim_{s\to 0} sC(s) \\ &= \lim_{s\to 0} \frac{s\left(H_o s^2 + D_o(t)s + K_o\right)}{H_o s^2 + D_o(t)s + K_o + K_{env} + \alpha K_{env}\dfrac{1-\Delta ts}{\Delta ts}} \frac{1}{s} = 0 \end{aligned} \tag{68}$$

So that with $t \to \infty$, $F_{env}(t) \to F_{env,d}(t)$.

4.4. More discussion for the stability analysis

Based on equation (43), we obtain

$$\begin{aligned} &\int_0^\infty \left(\sum_{i=1}^n \left({}^i\mathbf{V}_{i,r} - {}^i\mathbf{V}_i\right)^T \left({}^i\mathbf{V}_{i,r} - {}^i\mathbf{V}_i\right) \right) dt \\ &\le \frac{1}{\min(\lambda(\mathbf{K}_{D,i}))} \int_0^\infty \sum_{i=1}^n \left({}^i\mathbf{V}_{i,r} - {}^i\mathbf{V}_i\right)^T \mathbf{K}_{D,i} \left({}^i\mathbf{V}_{i,r} - {}^i\mathbf{V}_i\right) dt \\ &= \frac{1}{\min(\lambda(\mathbf{K}_{D,i}))} \left[{}^i\mathbf{V}_{i,r}(0) - {}^i\mathbf{V}_i(\infty) \right] \\ &\le \frac{1}{\min(\lambda(\mathbf{K}_{D,i}))} {}^i\mathbf{V}_{i,r}(0) \\ &< +\infty \end{aligned} \tag{69}$$

where $\min(\lambda(\mathbf{K}_{D,i}))$ denotes the minimum eigenvalue.

Based on the L_n^p definition yields

$$\left({}^i\mathbf{V}_{i,r} - {}^i\mathbf{V}_i\right) \in L_n^2 \cap L_n^\infty \tag{70}$$

Based on equation (70), we obtain

$$\lim_{t\to\infty} \left({}^i\mathbf{V}_{i,r} - {}^i\mathbf{V}_i\right) = \lim_{t\to\infty} \left(\dot{\mathbf{X}}_{e,r} - \dot{\mathbf{X}}_{e,d}\right) = 0 \tag{71}$$

Based on the Barbalet lemma, we get

$$\lim_{t\to\infty} \left(\ddot{\mathbf{X}}_{e,r} - \ddot{\mathbf{X}}_{e,d}\right) = 0 \tag{72}$$

Based on equation (72) and equation (24), the internal impedance control based on the internal force can be realized.

The instability of the inner loop control mainly comes from improper choices of the impedance parameters and VDC control gains, however, the choices of these

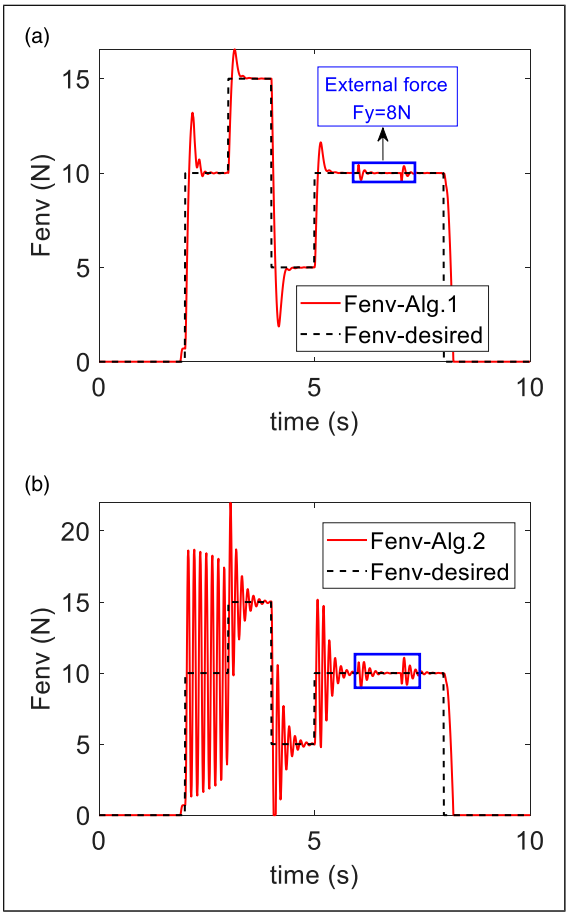

Figure 4. The force acting on the environment. (a) Algorithm 1. (b) Algorithm 2.

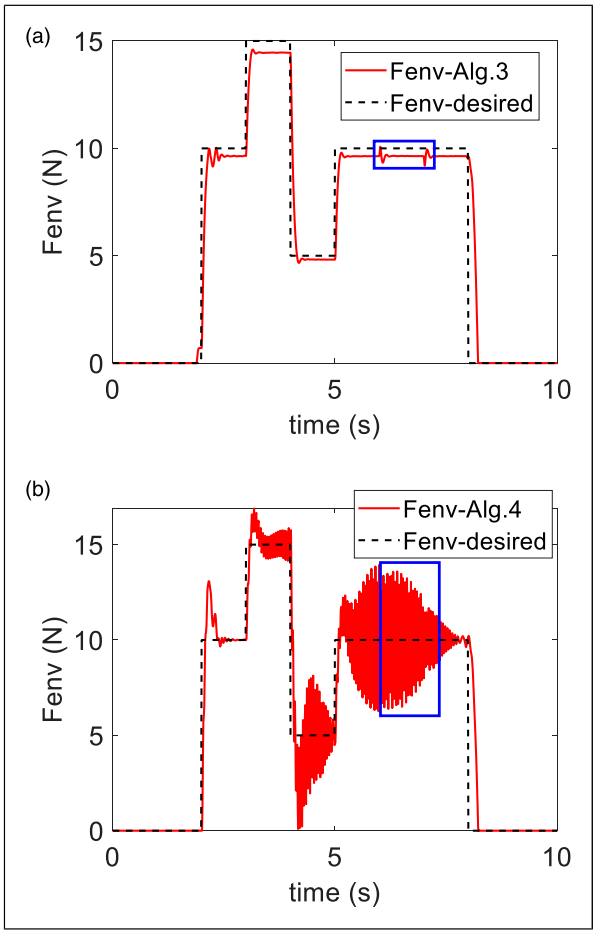

Figure 5. The force acting on the environment. (a) Algorithm 3. (b) Algorithm 4.

parameters are mainly dependent on the researchers' experience. A direct internal force control is embedded in the dual-loop control, so that the stiffness of the internal impedance control can be chosen relatively smaller. As for the instability of the outer loop control, if equation (67) does not satisfy, the contact force of the object with the environment will not converge to the desired contact force.

5. Simulation

The simulation model of this paper contains two rigid-joint robotic manipulators with a rigid object and the environment as Figure 3 shows:

The dual-arm system parameters are listed in Table 1.

The stiffness of the environment is $K_{env} = 8000\text{N/m}$ and the length of the environment is $L = 1$ m. The initial joint positions of the two arms are set as

$$\mathbf{q}_{0,a} = [\pi/3 + 0.1 \quad -2\pi/3 \quad -\pi/6] \text{ rad} \tag{73}$$

$$\mathbf{q}_{0,b} = [-\pi/3 \quad 2\pi/3 \quad \pi/6] \text{ rad} \tag{74}$$

The desired internal forces of the two arms acting on the end-effectors are set as

$$\mathbf{F}_{Id} = [25 \quad 0 \quad 0 \quad -25 \quad 0 \quad 0]^T \text{ N} \tag{75}$$

The desired contact force with the environment is set as

$$\begin{cases} F_{env,d} = 0 \text{ N} & 0 \le t < 2 \\ F_{env,d} = 10 \text{ N} & 2 \le t < 3 \\ F_{env,d} = 15 \text{ N} & 3 \le t < 4 \\ F_{env,d} = 5 \text{ N} & 4 \le t < 5 \\ F_{env,d} = 10 \text{ N} & 5 \le t < 8 \\ F_{env,d} = 0 \text{ N} & 8 \le t \le 10 \end{cases} \tag{76}$$

The trajectories are planned as the following form

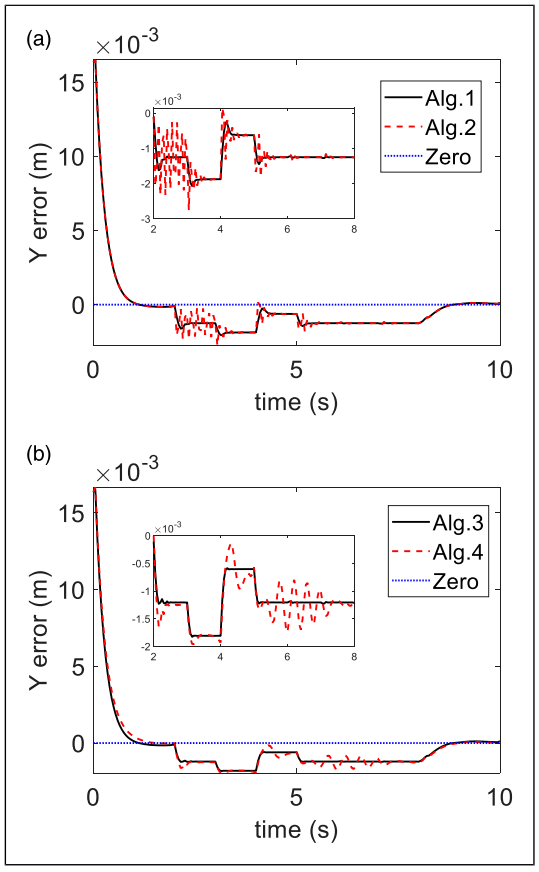

Figure 6. The position tracking errors in the Y direction. (a) Algorithm 1 and Algorithm 2. (b) Algorithm 3 and Algorithm 4.

$$
\begin{cases}
X_1 = \dfrac{x_2 - x_1}{T_1}\left[t - \dfrac{T_1}{2\pi}\sin\dfrac{2\pi}{T_1}\right] + x_1, \\
Y_1 = \dfrac{y_2 - y_1}{T_1}\left[t - \dfrac{T_1}{2\pi}\sin\dfrac{2\pi}{T_1}\right] + y_1, \\
\qquad 0 < \mathrm{t} \le 2 \\
X_2 = \dfrac{x_3 - x_2}{T_2}\left[(t-2) - \dfrac{T_2}{2\pi}\sin\dfrac{2\pi}{T_2}\right] + x_2, \\
Y_2 = \dfrac{y_3 - y_2}{T_2}\left[(t-2) - \dfrac{T_2}{2\pi}\sin\dfrac{2\pi}{T_2}\right] + y_2, \\
\qquad 2 < \mathrm{t} \le 8 \\
X_3 = \dfrac{x_1 - x_3}{T_3}\left[(t-8) - \dfrac{T_3}{2\pi}\sin\dfrac{2\pi}{T_3}\right] + x_3, \\
Y_3 = \dfrac{y_1 - y_3}{T_3}\left[(t-8) - \dfrac{T_3}{2\pi}\sin\dfrac{2\pi}{T_3}\right] + y_3, \\
\qquad 8 < \mathrm{t} \le 10
\end{cases}
\tag{77}
$$

where $(x_1, y_1) = (0.5, 1)$ m, $(x_2, y_2) = (0, 1.1)$ m, $(x_3, y_3) = (1, 1.1)$ m, $T_1 = T_3 = 2$ s, and $T_2 = 6$ s.

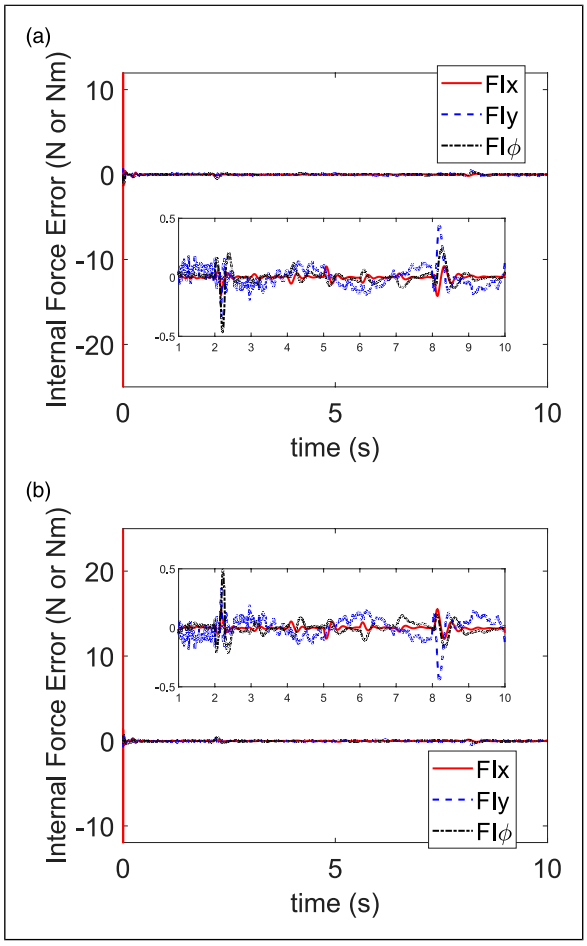

Figure 7. The internal force errors of the proposed algorithm1. (a) Arm-a. (b) Arm-b.

The sampling time is set as $\Delta t = 0.001$s, and the control gains are set as follows

$$
\begin{cases}
\mathbf{K}_{Di} = diag(80)_{3\times3}, \mathbf{P}_i = diag(1)_{13\times13} \\
\mathbf{K}_{lp} = diag(5)_{6\times6}, \mathbf{K}_{li} = diag(20)_{6\times6} \\
\mathbf{H}_d = diag(1)_{3\times3}, \mathbf{D}_d = diag(80)_{3\times3}, \mathbf{K}_d = diag(300)_{3\times3} \\
H_o = 3, K_o = 300, \alpha = 0.01, \beta = 20, d_0 = 10
\end{cases}
\tag{78}
$$

Adding the following friction disturbances in each joint as

$$\tau_{dis\_friction} = 2 \cdot sgn(\dot{q}_i) + 5 \cdot \dot{q}_i \tag{79}$$

Adding the time-varying disturbances in each joint as

$$\tau_{dis} = 5 \cdot \sin(t) + 10 \cdot \sin(2t) \tag{80}$$

Adding the external force disturbance in the Y direction of the object as

$$F_{dis,y} = 8 \text{ N} \quad \mathrm{t} = [6, 7]\mathrm{s} \tag{81}$$

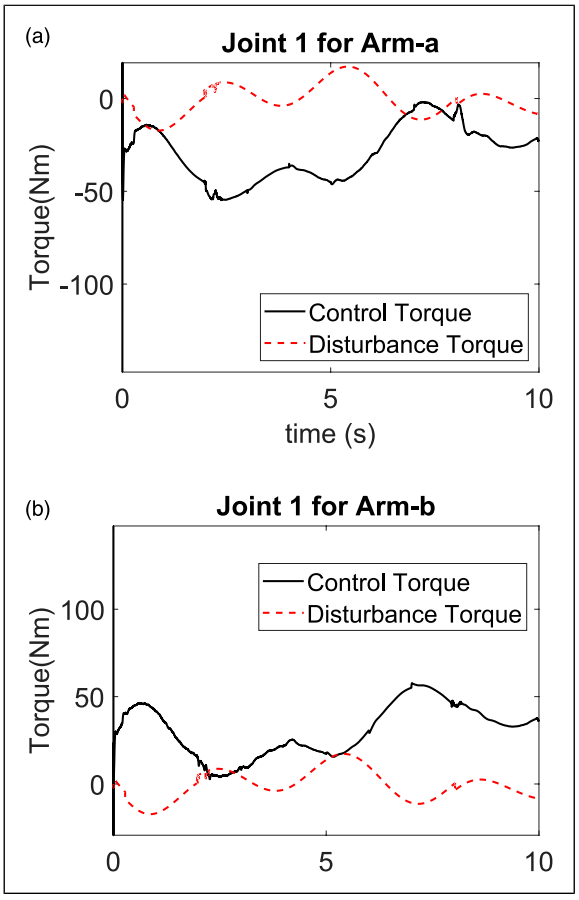

Figure 8. The control torque and disturbance torque of joint 1 for Arm-a and Arm-b (a) The torque of joint 1 for Arm-a. (b) The torque of joint 1 for Arm-b.

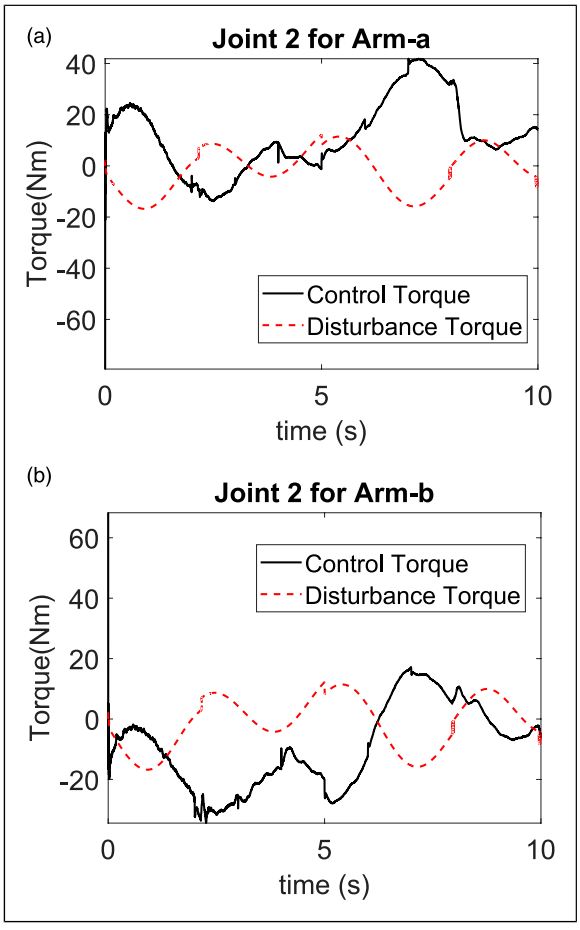

Figure 9. The control torque and disturbance torque of joint 2 for Arm-a and Arm-b (a) The torque of joint 2 for Arm-a. (b) The torque of joint 2 for Arm-b.

To present the control effectiveness by a comparison, four algorithms are set as follows:

Algorithm1. the proposed control scheme in this paper.
Algorithm2. compared with Algorithm1, close the dynamic damping of the outer-loop impedance control, and set $D_o = 2\sqrt{K_o H_o}$.
Algorithm3. compared with Algorithm1, close the adaptive stiffness.
Algorithm4. compared with Algorithm1, close the adaptive parameters in the low-level position control of the VDC.

Based on the above four cases, the force exerted on the environment is shown in Figures 4 and 5.

Observing from Figure 4(a) and Figure 4(b), the contact force of the Algorithm 1 has an obvious advantage compared with the Algorithm 2, due to the dynamics damping action in the Algorithm 1. Observing from Figure 5(a), Algorithm 3 has different force deviations using the invariable impedance parameters, the bigger the stiffness of the outer impedance, the bigger the force deviation. Observing from Figure 5(b), without the parameter adaptation of the Algorithm 4 in the low-level VDC method, the vibration of the object is always existing in the contact stage with the environment, the adaptation in the VDC can effectively reduce the PD gains in the low-level position control.

The position tracking errors for the Y direction in the base frame are shown in Figure 6.

In the non-contact stage of the object with the environment, $[0 \sim 2]$s and $[8 \sim 10]$s, the higher position tracking precision is obtained, however, in the contact stage $[2 \sim 8]$s, the desired contact force is required, so an obvious position deviation is arisen in the Y direction.

The above four algorithms used the same internal force control method, so that the internal force tracking error has very little difference. Therefore, only the internal force error of the proposed control scheme is shown in Figure 7, including Arm-a and Arm-b. Observing from Figure 7, to guarantee a steady grasp, a faster internal force convergence speed is obtained. The internal force obtained from the force sensor is added with the white noise, however, after the Kalman filter, the force deviation is within ±0.5 N, which is acceptable with the real robotic task.

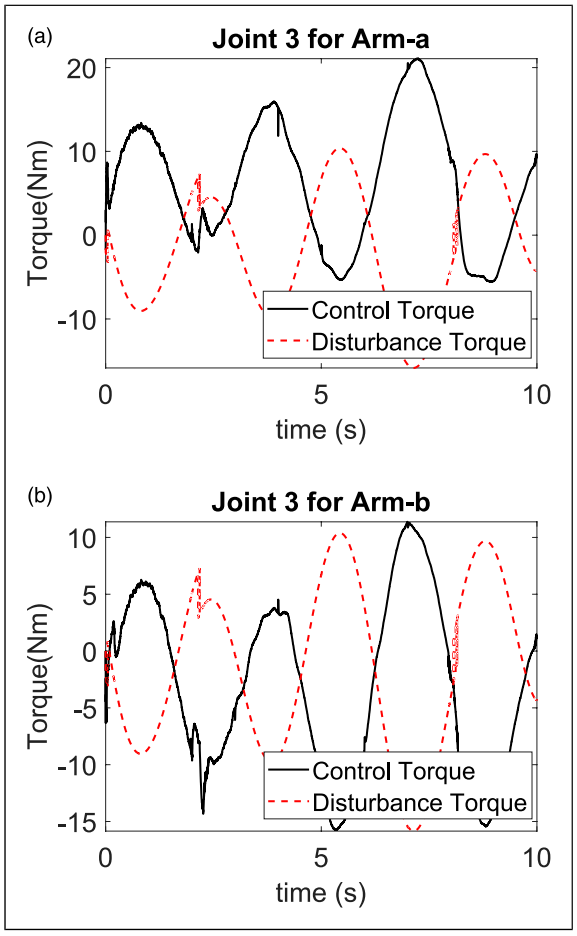

Figure 10. The control torque and disturbance torque of joint 3 for Arm-a and Arm-b (a) The torque of joint 3 for Arm-a. (b) The torque of joint 3 for Arm-b.

The control torque and disturbance torque of each joint for Arm-a and Arm-b are shown in Figures 8 to 10.

6. Conclusion

The modified dual-loop variable impedance control scheme proposed in this paper can meet multi control requirements simultaneously, including the external/internal force tracking control, and the position tracking control of the object. The proposed adaptive impedance can effectively copy with the unknown stiffness and position of the environment. The additional dynamic adjustment of the damping can reduce the vibration of the object in the contact stage. The incorporation of the VDC in the low-level position control allows the dynamics of the two arms are unknown. And because of the feedforward compensation due to the adaptation in the VDC, the amplitude of the "PD" controller can be decreased largely, so that the stability and robustness can be improved.

The limitations and challenges are reflected in two aspects in the practical applications: one is that all the forces are assumed that they can be measured from the force sensors, usually the internal force can be measured from the force sensors located in the end-effectors, however, the force between the object and the environment cannot be measured directly, some force estimation methods can be used in the practical applications. The other is that the position and force tracking performances are effected largely by the kinematics of the system, including the kinematics of the two arms and the object, some adaptive controllers considering the kinematics uncertainties have been proposed, however, these methods rely on the vision measurement.

Declaration of conflicting interests

The author(s) declared no potential conflicts of interest with respect to the research, authorship, and/or publication of this article.

Funding

The author(s) received no financial support for the research, authorship, and/or publication of this article.

ORCID iDs

Xin Jing https://orcid.org/0000-0003-4874-7253
Loris Roveda https://orcid.org/0000-0002-4427-536X
Yaobing Wang https://orcid.org/0000-0002-0363-0580

References

Babarahmati KK, Tiseo C, Rouxel Q, et al. (2021) *Robust and Dexterous Dual-Arm Tele-Cooperation Using Fractal Impedance Control*. arXiv preprint arXiv:2108.04567.

Bonitz R and Hsia TC (1996)a Internal force-based impedance control for cooperating manipulators. *IEEE Transactions on Robotics and Automation* 12: 78–89.

Bonitz RG and Hsia TC (1996b) Robust internal-force based impedance control for coordinating manipulators-theory and experiments. In: Proceedings of the IEEE international conference on robotics and automation, Minneapolis, MN, USA, 22–28 April 1996. IEEE, pp. 622–628.

Caccavale F, Chiacchio P, Marino A, et al. (2008) Six-dof impedance control of dual-arm cooperative manipulators. *IEEE/ASME Transactions On Mechatronics* 13: 576–586.

Caccavale F and Uchiyama M (2016) Cooperative manipulation. *Springer Handbook of Robotics*. Berlin: Springer.

Dong S and Mills JK (2002) Adaptive synchronized control for coordination of multirobot assembly tasks. *IEEE Transactions on Robotics and Automation* 18: 498–510.

Erickson D, Weber M and Sharf I (2003) Contact stiffness and damping estimation for robotic systems. *The International Journal of Robotics Research* 22: 41–57.

Ferraguti F, Secchi C and Fantuzzi C (2013) *A tank-based approach to impedance control with variable stiffness*. In: Proceedings of the 2013 IEEE international conference on robotics and automation, Karlsruhe, Germany, 06-10 May 2013. IEEE, 4948–4953.

He J, Luo M and Zhang Q (2016) *Dual impedance control with variable object stiffness for the dual-arm cooperative manipulators*. In: Proceedings of the 2016 Asia-Pacific conference on intelligent robot systems (ACIRS), Tokyo, Japan, 20-22 July 2016. IEEE, pp. 102–108.

Heck D, Kostić D, Denasi A, et al. (2013) *Internal and external force-based impedance control for cooperative manipulation*. In: Proceedings of the 2013 European control conference (ECC), Zurich, Switzerland, 17-19 July 2013. IEEE, pp. 2299–2304.

Hu H and Cao J (2022) Adaptive variable impedance control of dual-arm robots for slabstone installation. *ISA Transactions* 128: 397–408.

Jiao C, Yu L, Su X, et al. (2022) Adaptive hybrid impedance control for dual-arm cooperative manipulation with object uncertainties. *Automatica* 140: 110232.

Jinjun D, Yahui G, Ming C, et al. (2019) Symmetrical adaptive variable admittance control for position/force tracking of dual-arm cooperative manipulators with unknown trajectory deviations. *Robotics and Computer-Integrated Manufacturing* 57: 357–369.

Khalil HK (1996) Adaptive output feedback control of nonlinear systems represented by input-output models. *IEEE Transactions on Automatic Control* 41: 177–188.

KoivumäKI J and Mattila J (2017) Stability-guaranteed impedance control of hydraulic robotic manipulators. *IEEE/ASME TransactiOns on MechatrOnics* 22: 601–612.

Li J, Wang Y, Liu Z, et al. (2021) *A New Recursive Composite Adaptive Controller for Robot Manipulators*. Beijing, China: Space: Science and Technology.

Lin HC, Smith J, Babarahmati KK, et al. (2018) A projected inverse dynamics approach for multi-arm cartesian impedance control. In: Proceedings of the IEEE international conference on robotics and automation (ICRA), Brisbane, QLD, Australia, 21-25 May 2018. IEEE, pp. 5421–5428.

Lin T and Goldenberg AA (1997) On coordinated control of multiple flexible joint robots holding a constrained object. In: Proceedings of the international conference on robotics and automation, Albuquerque, NM, USA, 25 April 1997. IEEE, pp. 1490–1495.

Luh J and Zheng Y (1987) Constrained relations between two coordinated industrial robots for motion control. *The International Journal of Robotics Research* 6: 60–70.

Ping H (1992) Coordinated control of multiple manipulator systems. *IEEE Transactions on Robotics and Automation* 9: 400–410.

Ren Y, Liu Y, Jin M, et al. (2016) Biomimetic object impedance control for dual-arm cooperative 7-DOF manipulators. *Robotics and Autonomous Systems* 75: 273–287.

Rodriguez-Angeles A and Nijmeijer H (2004) Mutual synchronization of robots via estimated state feedback: a cooperative approach. *IEEE Transactions on Control Systems Technology* 12: 542–554.

Roveda L and Piga D (2020) Robust state dependent Riccati equation variable impedance control for robotic force-tracking tasks. *International Journal of Intelligent Robotics and Applications* 4: 507–519.

Shahriari E, Birjandi SAB and Haddadin S (2022) Passivity-based adaptive force-impedance control for modular multi-manual object manipulation. *IEEE Robotics and Automation Letters* 7: 2194–2201.

Smith C, Karayiannidis Y, Nalpantidis L, et al. (2012) Dual arm manipulation—a survey. *Robotics and Autonomous Systems* 60: 1340–1353.

Song X, Mao H, Huang H, et al. (2021) *A dynamic adaptive impedance controller for force tracking of dual-arm manipulators in uncertain contact environment*. In: Proceedings of the IEEE international conference on robotics and biomimetics (ROBIO), Sanya, China, 27-31 December 2021. IEEE, 1674–1681.

Uchiyama M and Dauchez P (1988) A symmetric hybrid position/force control scheme for the coordination of two robots. In: Proceedings of the IEEE international conference on robotics and automation, Philadelphia, PA, USA, 24-29 April 1988.

Walker ID, Freeman RA and Marcus SI (1991) Analysis of motion and internal loading of objects grasped by multiple cooperating manipulators. *The International Journal of Robotics Research* 10: 396–409.

Wang Y (2021) *Space Robotics*. Berlin: Springer.

Weng CY, Tan WC and Chen I (2019) A survey of dual-arm robotic issues on assembly tasks. *ROMANSY 22–Robot Design, Dynamics and Control* 584: 474–480. Springer.

Zhai A, Wang J, Zhang H, et al. (2022) Adaptive robust synchronized control for cooperative robotic manipulators with uncertain base coordinate system. *ISA Transactions* 126: 134–143.

Zhu WH (2010) *Virtual Decomposition Control: Toward Hyper Degrees of Freedom Robots*. Berlin: Springer Science and Business Media.

Zhu WH, Bien Z and De Schutter J (1998) Adaptive motion/force control of multiple manipulators with joint flexibility based on virtual decomposition. *IEEE Transactions on Automatic Control* 43: 46–60.

Zhu WH and De Schutter J (1999) Control of two industrial manipulators rigidly holding an egg. *IEEE Control Systems Magazine* 19: 24–30.

Zhu WH and De Schutter J (2002) Experimental verifications of virtual-decomposition-based motion/force control. *IEEE Transactions on Robotics and Automation* 18: 379–386.